FISEVIER

# Contents lists available at ScienceDirect

# Powder Technology

journal homepage: www.journals.elsevier.com/powder-technology



# Short Communication



# Automated dynamic image analysis for particle size and shape classification in three dimensions

Sadegh Nadimi a,b,\*, Vasileios Angelidakis c,b, Sadaf Maramizonouz a, Chao Zhang a

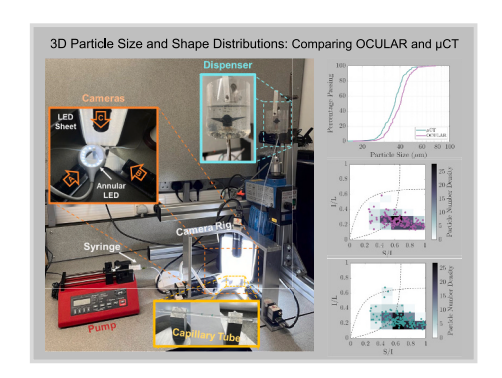
- <sup>a</sup> School of Engineering, Newcastle University, Newcastle upon Tyne, United Kingdom
- <sup>b</sup> Ocular Systems Ltd., Newcastle upon Tyne, United Kingdom
- <sup>c</sup> School of Natural and Built Environment, Queen's University Belfast, Belfast, United Kingdom

# HIGHLIGHTS

# We introduce OCULAR, a 3D dynamic image analysis for micron-sized particle characterisation.

- OCULAR outperforms 2D methods by capturing the full particle morphology, improving accuracy.
- The repeatability of OCULAR is verified via consistent characterisation results.
- Agreement of OCULAR with μCT highlights its reliability for particle analysis.

# GRAPHICAL ABSTRACT



# ARTICLE INFO

# Keywords: Dynamic image analysis 3D image reconstruction Particle size Particle shape

# ABSTRACT

We introduce OCULAR, an innovative hardware and software solution for three-dimensional dynamic image analysis of micron-sized particles. Current state-of-the art instruments for dynamic image analysis are largely limited to two-dimensional imaging. However, extensive literature has demonstrated that relying on a single two-dimensional projection for particle characterisation can lead to inaccuracies in many applications. Existing three-dimensional imaging technologies, such as computed tomography, laser scanning, and orthophotography, are limited to static objects. These methods are often not statistically representative and come with significant post-processing requirements, as well as the need for specialised imaging and computing resources. OCULAR addresses these challenges by providing a cost-effective solution for imaging continuous particle streams using a synchronised array of optical cameras. Particle shape characterisation is achieved through the reconstruction of their three-dimensional surfaces. This paper details the OCULAR methodology, evaluates its repeatability, and reliable particle analysis.

<sup>\*</sup> Corresponding author at: School of Engineering, Newcastle University, Newcastle upon Tyne, United Kingdom. *E-mail address:* sadegh.nadimi-shahraki@ncl.ac.uk (S. Nadimi).

# 1. Introduction

Particle size and shape are essential characteristics of particulate materials significantly influencing their behaviours and interactions with their surroundings across diverse applications such as food industry [1,2], cell biology [3], pharmaceutical tableting [4], transport [5], and even space exploration [6].

Conventionally, particle shape characterisation has relied on twodimensional (2D) analysis of particle projections using microscopy techniques. While 2D shape characterisation could provide valuable insights particularly for general shape or size distribution, it may not be adequate as it inherently overlooks the particle third dimension causing unrealistic assumptions. This can result in limitations when translating findings from 2D representations to real-world applications particularly where the full 3D shape impacts material interactions, flow dynamics, or structural stability [7].

In response, three-dimensional (3D) characterisation has emerged as a more comprehensive method [8,9]. By capturing the full morphology, 3D particle shape characterisation enables a deeper understanding of particle behaviour in various contexts. The imaging technologies currently available for 3D imaging such as computed tomography, laser-scanning, electron microscopy and orthophotography offer high accuracy but come with considerable challenges. These systems require substantial investment in both equipment and data processing time and are often limited to static and small sample sizes, restricting their applicability for real-time analyses that demand rapid, large-scale assessments, such as in processing or production settings [7].

To address these limitations, the current work proposes a novel and cost-effective hardware and software solution for the 3D dynamic image acquisition and shape characterisation of particles, focusing on wet dispersion. In this system, a continuous flow of a fluid-particles suspension is recorded using a set of synchronised optical cameras. Then, particle morphology, i.e. size and shape, is characterised by reconstructing the real 3D particle geometry. The present setup delivers a more realistic representation of particle morphology compared to 2D dynamic image analysis solutions, enhancing the accuracy and applicability of shape characterisations across various fields involving micron-sized particles. Moreover, the OCULAR system is applicable beyond wet dispersion, and can handle dry samples with suitable dispersion units, offering broader adaptability.

# 2. Methods

# 2.1. Components of OCULAR

OCULAR comprises optical imaging components, connected to and controlled by a central computing unit which is also used for synchronised image acquisition of the 2D projections, for a faster way of 3D reconstruction and subsequently for particle characterisation and classification. In the current work, three orthogonally positioned optical cameras (IDS U3-3040CP Rev.2.2) with a resolution of 1.58 megapixels (1456  $\times$  1088 pixels), a pixel size of 3.45  $\mu m$ , and a frame rate of up to 251 frames per second are used. Each camera is connected with a lens (IDS-20 M11-C7528), featuring a 75 mm focal length with a resolution of up to 20.50 megapixels. The cameras and lenses are mounted on a rig and the cameras are then connected to an interface card of a workstation via USB 3.0 cables. Each lens is positioned 80 mm away from the particles flowing through a square capillary tube (Hollow Square Capillaries, Part Number 8100–100, CM Scientific, UK) with a 1 mm  $\times$  1 mm cross-section and a 100 mm length, mounted on the same rig in front of the three cameras. A study on camera arrangement and the number of cameras found no objectively preferable configuration. The current setup is effective in terms of fabrication and data processing, as it requires the minimum number of cameras.

The OCULAR system is constrained by the resolution limit of the optical microscopy, which is approximately 200 nm. To ensure accurate

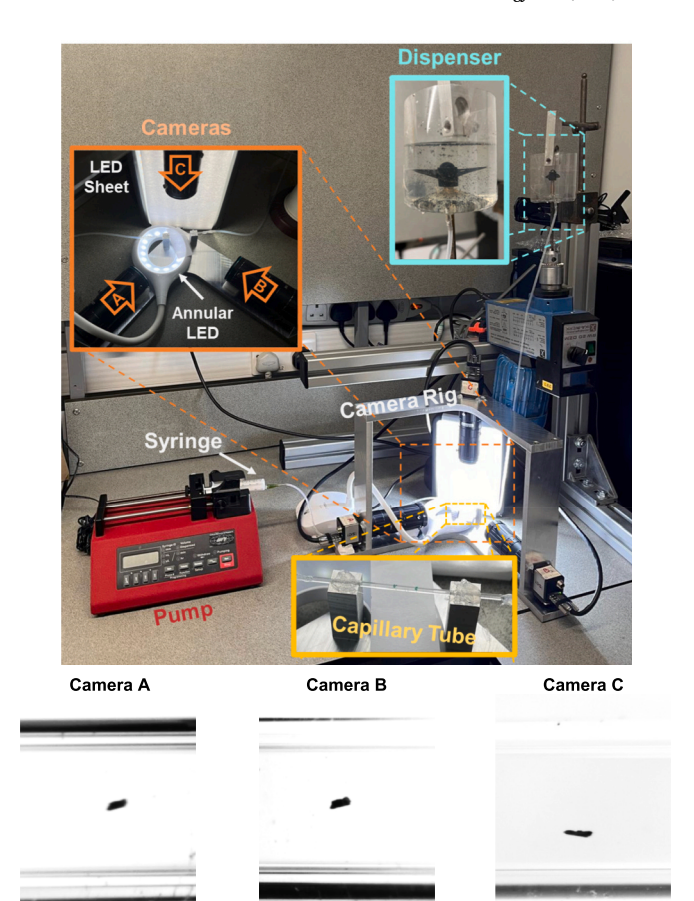


Fig. 1. An outline of the OCULAR set-up, demonstrating the camera arrangement, dispensing unit, illumination, and the capillary tube.

size measurements, a minimum of 10 pixels across the particle diameter is recommended, making the suitable size range for analysis above 2  $\mu m$ . For shape characterisation, certain indices require more pixels across the particle diameter, typically in the range of 2–4  $\mu m$ , depending on the parameter [10]. These constraints ensure reliable measurements for both size and shape analysis within this range.

The region of interest (RoI) for the imaging is illuminated by two LED lights, a rectangular LED light placed at the back of the camera rig and an annular LED light placed below the capillary tube. The square capillary is connected to a syringe pump (Aladdin AL-1000 SyringeONE Programmable Syringe Pump) using flexible tubing (RS PRO Silicone Stock No.273–2490, RS Components Ltd., UK) with inner and outer diameters of 1.5 mm and 2.5 mm, respectively. Fig. 1 shows an outline of the OCULAR set-up.

# 2.2. Image acquisition of dynamic objects

A fluid-particle suspension is made by mixing 37.3 micrograms of alumina particles (L.B. Foster Rail Technologies, UK) in a solution of 0.1 g of Xanthan powder (Xanthan gum from Xanthomonas campestris, Sigma Aldrich, UK) to 100 g deionised (DI) water. The alumina particles, with a nominal size range of 63–75  $\mu m$ , were obtained through sieve analysis. Xanthan gum is used due to its viscoelastic and shear-thinning properties, which help maintain a stable particle suspension and facilitate controlled flow through the fluidic system, reducing particle aggregation during imaging [11]. The suspension is pumped and/or withdrawn through the fluidic system using the syringe pump with a set flow rate. This process is automated, where particles are fed into the dispenser, and subsequent steps are performed seamlessly. Two containers are utilised at each of the fluidic system: one for containing the fluid-particle

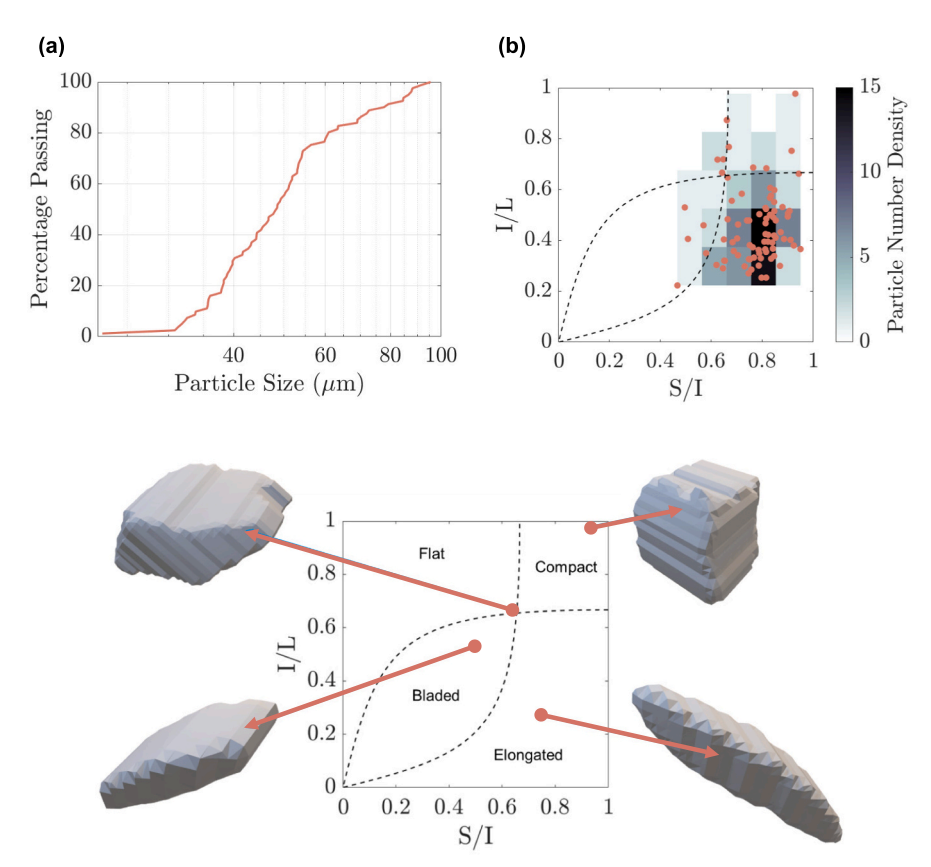


Fig. 2. The (a) particle size distribution of the alumina particles, and (b) particle shape distribution of the alumina sample presented on a Zingg [10] chart and coloured by the particle number density.

sample which is constantly stirred using a mixer (RW 20 DZM, IKA Werke GmbH Janke & Kunkel, Germany) to avoid sedimentation of the alumina particles, and the other for collecting the output of the system (Fig. 1). The fluid-particle suspension flows through the flexible tubing and then the square capillary. The three cameras capture synchronised videos of the three views of each particle as they enter and exit the RoI. Fig. 1 is annotated to better illustrate the process of the OCULAR system. Three synchronised 2D projections of each individual particle are extracted from the videos and then processed for the 3D reconstruction of particle shape.

# 2.3. Dynamic calibration

Before conducting the tests, the optical imaging system is calibrated by capturing three images of sapphire precision spheres (Sapphire Balls Product Code: AL66-SP-000105, Goodfellow, USA) with a diameter of 250  $\mu m$  and manufacturing tolerance of 2.5  $\mu m$ , which is suspended in the same Xanthan-water solution and sealed inside a square capillary. The three 2D projections are then compared to the geometry of the sapphire precision spheres produced to calibrate the three cameras.

# 2.4. Principles and significance of the 3D-reconstruction technique

Each 2D projection is captured initially as a grayscale image. These projections are then binarised to isolate particle images (black and white image), and denoising is used to remove any isolated pixels, ensuring that a single object is identified in each image, corresponding to the particle projection. Volume extrusion is performed along the respective axes of the 2D projections, and the common volume is determined by intersecting these extrusions to reconstruct the 3D morphology of particle. This process is implemented using an in-house MATLAB algorithm specifically developed for the OCULAR system.

Even though measuring the real convexity of the particle accurately is at risk following this reconstruction approach, the overall form in terms of flatness and elongation is still represented well, if a minimal bounding box is used to estimate the main particle dimensions, since this is not affected by convexity. By definition, a particle and the convex hull of the particle share the same minimal bounding box and thus main dimensions. This reconstruction approach can capture concavities, as concave features visible in one or more projections are reflected in the extruded volumes and incorporated into the final 3D shape. In addition, relevant validation experiments were performed to compare the reconstructed shapes with µCT data and are shown in the Results and Discussion section. However, for particles with complex internal or hidden concavities, this method will not capture such features. This ability to capture particle form positions the system in significant advantage compared to 2D image characterisation instruments, which rely solely on a single projection of the particle, risking the failure of capturing both convexity and form.

A 2D image of a particle cannot represent whether a particle is compact, flat, elongated, or bladed (flat and elongated), as there is no information of what is happening in the other direction. As a result, a particle might look compact in a 2D image but be elongated in reality or look elongated in a 2D image but be flat in reality. 3D objects can only be imaged adequately using 3D information, as inferring their characteristics from a single perspective bears a significant amount of ambiguity on the actual particle geometry. Hollow particles, or particles with concealed concavities, which cannot be captured from perimetric images, can be imaged using laser scanning (if the particle orientation allows) or using x-ray micro computed tomography regardless of particle orientation, but both methods require the particle to be static for prolonged amounts of imaging time, and do not allow the imaging of continuous streams of particles. The OCULAR system presented here, by combining orthogonal projections and 3D reconstruction, eliminates the

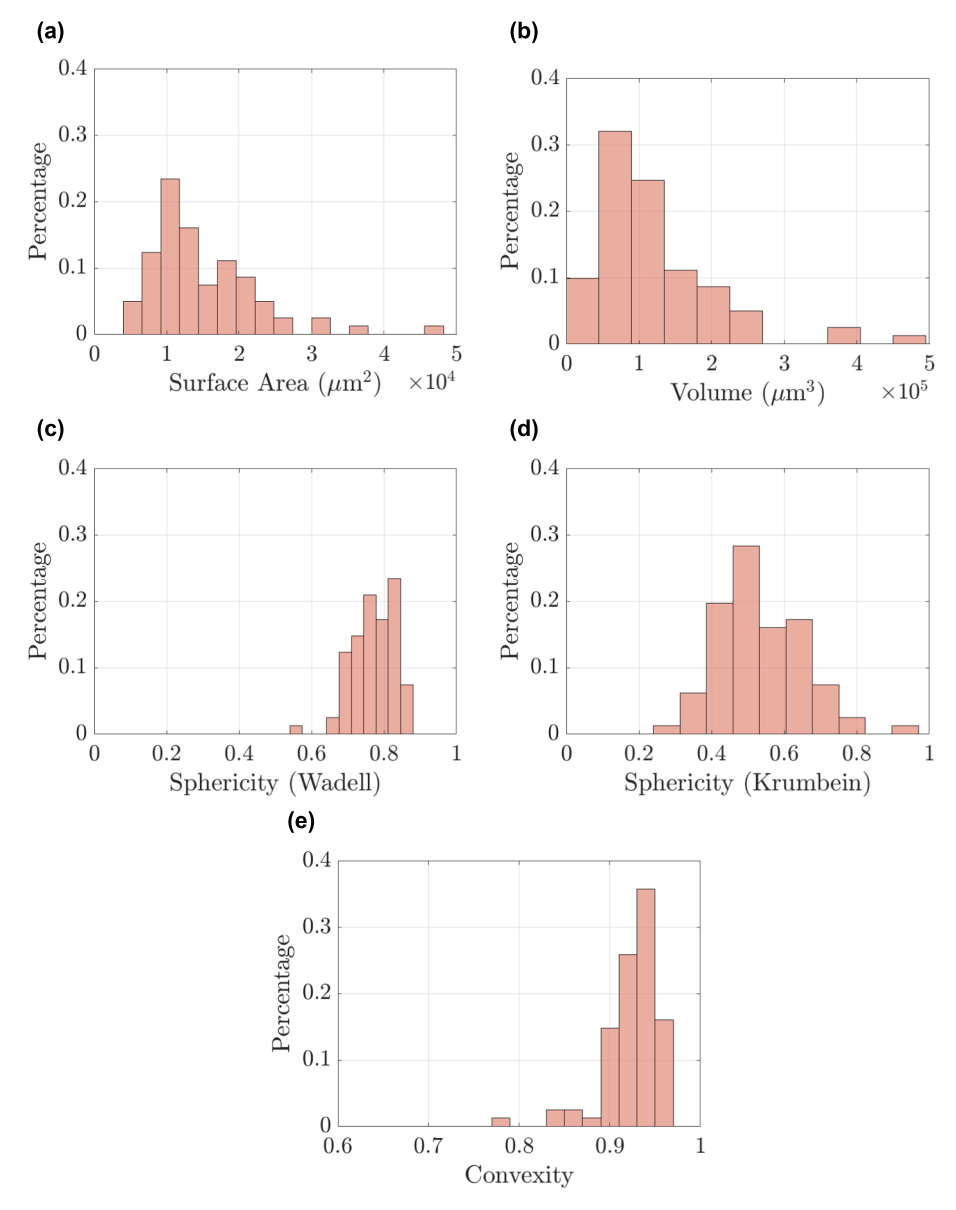


Fig. 3. The particles (a) surface area, (b) volume, (c) true sphericity [12], (d) intercept sphericity [13], and (e) convexity of the alumina sample.

ambiguity of 2D imaging while offering efficient 3D analysis of particles in high throughput flow with capturing essential morphological characteristics of particles.

# 2.5. How to describe size and shape in 3D

In 3D analysis, particle size is typically characterised through dimensions along orthogonal axes, allowing for comprehensive representation of particle dimension. A common approach is using a bounding box which defines a rectangular prism tightly enclosing the particle, and capturing its short (S), intermediate (I), and long (L) dimensions in three perpendicular directions. The intermediate dimension has been used to represent the particle size. Additionally, other metrics like volume and surface area are utilised for 3D size characterisation [12].

Characterising particle shape in three dimensions requires indices that capture the morphology adequately, focusing on shape descriptors such as elongation, flatness, compactness, and sphericity. The Zingg shape classification system [13] is one of the foundational methods for categorising particle shape, utilising the values of particle flatness and elongation to classify particles into for shape categories of compact, flat,

elongated, and bladed. In the Zingg chart, the elongation index is defined as the ratio of a particle intermediate to long dimensions (I/L), while the flatness index is defined as the ratio of the particle short to intermediate dimensions (S/I). By combining multiple shape descriptors, researchers can achieve a detailed and consistent representation of particle morphology, facilitating accurate modelling in various applications. To address the limitations of the traditional Zingg system, a recently proposed system [12] introduced non-linear boundaries for I/L and S/I indices. These updated boundaries improve the classification of particles, especially those with extreme aspect ratios, and have been validated for diverse particle shapes.

# 3. Results and discussion

The size and shape of 81 alumina particles are characterised using the OCULAR system and the SHAPE code [14]. Fig. 2 shows (a) the Particle Size Distribution (PSD) based on the particle intermediate dimension and (b) the shape distribution of the particles plotted on a Zingg chart [13] and coloured by the particle number density which represents the relative frequency of particles in specific regions of the chart and is dimensionless, as it is calculated as a ratio of particle counts

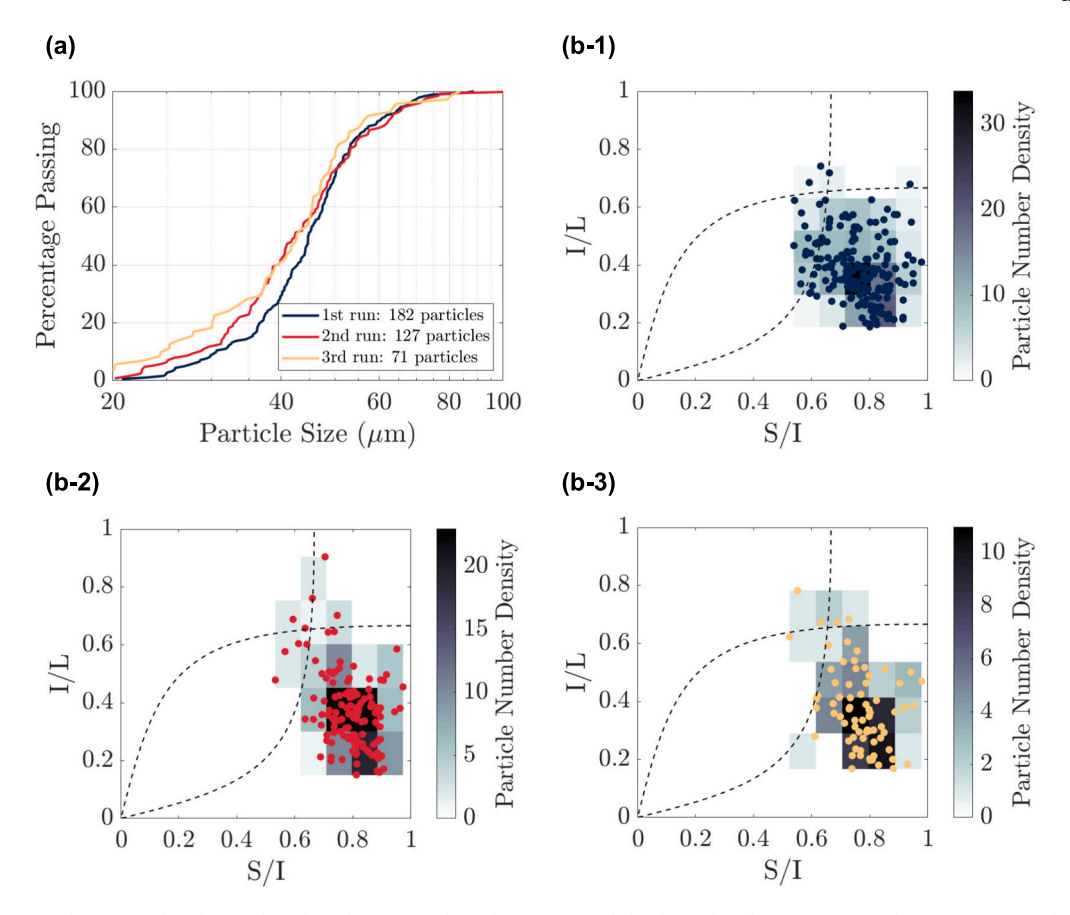


**Fig. 4.** The alumina particle (a) size distribution based on the intermediate dimension, and (b) shape distribution (presented on a Zingg [10] chart and coloured by the particle number density) for the (1) first, (2) second, and (3) third run of the same sample during the repeatability study.

to the total number of particles. It can be seen that the majority of particles belong to the elongated shape category. The particles surface area, volume, true sphericity [15], intercept sphericity [16], and convexity [17] are presented in Fig. 3(a) to (e).

# 3.1. Repeatability of results

The repeatability of the OCULAR system is quantified by characterising the same fluid-particle suspension sample of alumina in a 0.2 g to 100 g solution of Xanthan powder and DI water, which is prepared and run through the system three times. The alumina powder was sieved, and particles retained between 63 and 75 µm were collected. For each run of the same sample, the three cameras capture synchronised videos of the three views and individual particles are 3D reconstructed and characterised. The number of 182, 127, and 71 alumina particles are identified and characterised for the first, second, and third run of the experiment, respectively. A loss of 55 and 56 particles occurs between the first and second, and the second and third runs of the repeatability experiments, respectively. This loss is primarily due to some particles remaining in the system, particularly in syringes, or in the capillary tube, where adhesion or gravity-driven effects may prevent complete flushing. Additionally, small and irregularly shaped particles may settle or adhere to internal surfaces at the end of each run. Minor operational variations can also contribute to these losses. Despite this, the number of particles analysed in the repeatability tests falls within the range suggested by previous studies for reliable particle size distribution analysis [18].

Fig. 4 demonstrates that the particle size and shape distribution data obtained from the three runs remain highly consistent, highlighting the system provides repeatable and statistically robust measurements. In particular, Fig. 4(a) illustrates that the measurement of particle size distribution is highly consistent throughout the three runs of the

repeatability study with a slight discrepancy for particles smaller than 40  $\mu$ m. Fig. 4(b-1) to (b-3) show the particle shape distributions for the three runs which confirm the consistency of the measurement, also, in terms of particle shape.

# 3.2. Comparison with $\mu$ CT

The size and shape distributions of 154 alumina particles, obtained through  $\mu$ CT and the OCULAR, are presented in Fig. 5(a), (b-1), and (b-2). The same set of 154 particles was used for both methods, ensuring direct comparability. The particles were first scanned using  $\mu$ CT for detailed size and shape analysis and then analysed using the OCULAR system. Shape characterisation is performed using the SHAPE code [14]. The particle size distribution data in Fig. 5(a) demonstrate good agreement between the  $\mu$ CT and OCULAR results, with the latter slightly overestimating particle sizes. The overestimation may result from the OCULAR system's reconstruction approach, where 3D particles are generated by extruding 2D projections. This process can slightly enlarge particle dimensions due to the inclusion of surface roughness or concave features. Fig. 5(b-1) and (b-2) compares the particle shape distributions from  $\mu$ CT and OCULAR, revealing that OCULAR provides a classification that closely matches that of  $\mu$ CT.

The comparison between the particle size from both  $\mu$ CT and OCULAR versus their corresponding I/L and S/I values are shown in Fig. 5(c) and (d), respectively. Both graphs show the majority of the data points overlap with only a few discrepancies.

To analyse the agreement between  $\mu CT$  and OCULAR, two Bland-Altman plots for values of I/L and S/I are presented in Fig. 5(e) and (f), respectively. Both graphs show overall good agreement between  $\mu CT$  and OCULAR, with no major systematic bias. The presence of a few outliers suggests that the methods may not always be interchangeable in

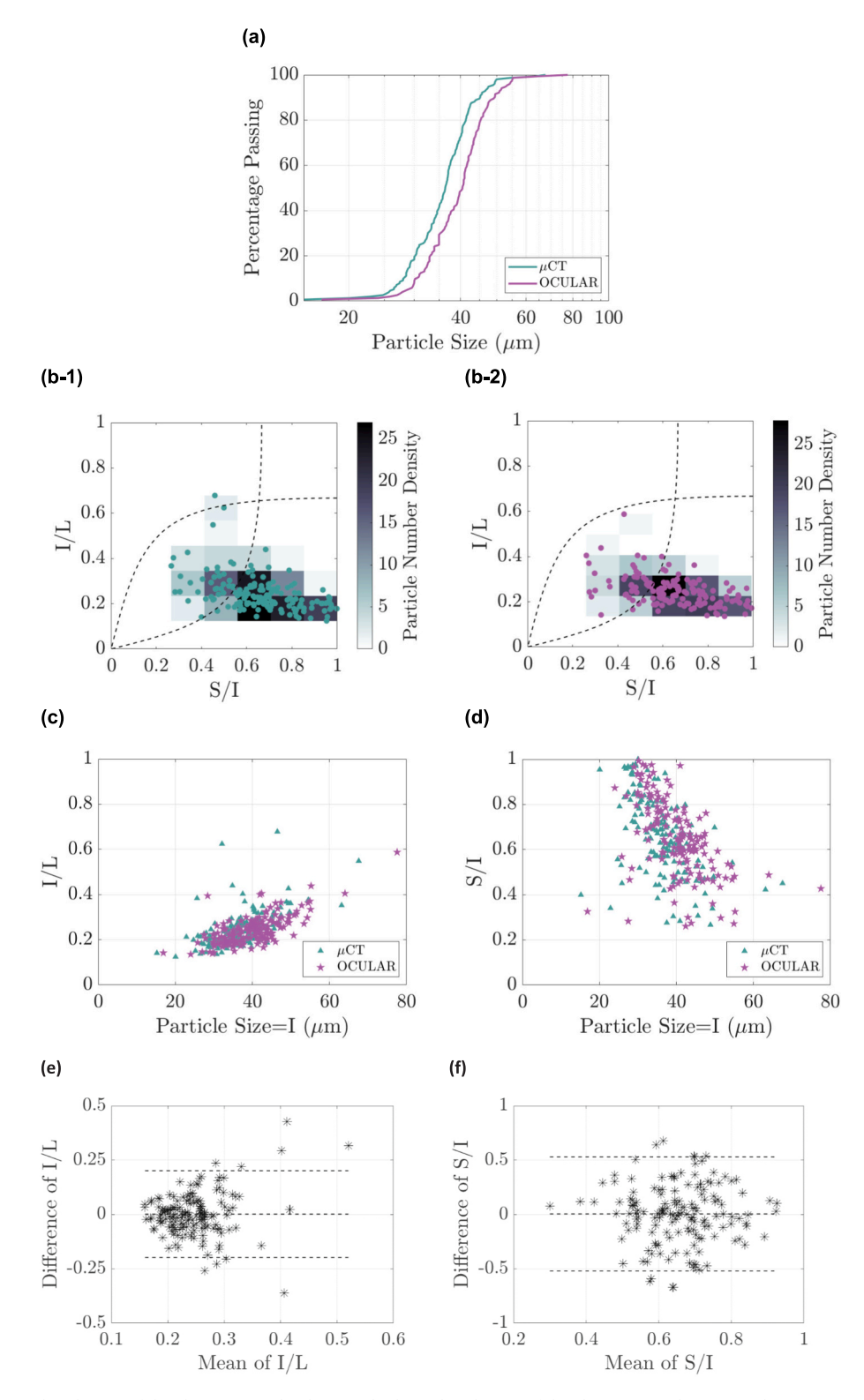


Fig. 5. The (a) particle size distribution of the alumina sample, (b) particle shape distribution of the alumina sample presented on a Zingg [10] chart and coloured by the particle number density obtained through (1)  $\mu$ CT, and (2) OCULAR, (c) I/L versus particle size(I), (d) S/I versus particle size(I), (e) Bland-Altman graph of the I/L, and (f) Bland-Altman graph of the S/I.

# extreme cases.

Comparisons between the particles surface area, volume, true sphericity [15], intercept sphericity [16], and convexity [17] obtained through both  $\mu CT$  and OCULAR are presented in Fig. 6(a) to (e). As previously discussed, OCULAR can slightly overestimate the particle convexity evident in Fig. 6(e). This overestimation in convexity can

result in the overestimation of particle volume and underestimation of particle surface area as shown in Fig. 6(a) and (b), respectively. The particles intercept sphericity [13] remains similar for both methods as shown in Fig. 6(d) due to the use the particles short, intermediate, and long dimensions in its calculations, whereas the particles true sphericity [12] is overestimated by OCULAR as shown in Fig. 6(c) due to the use

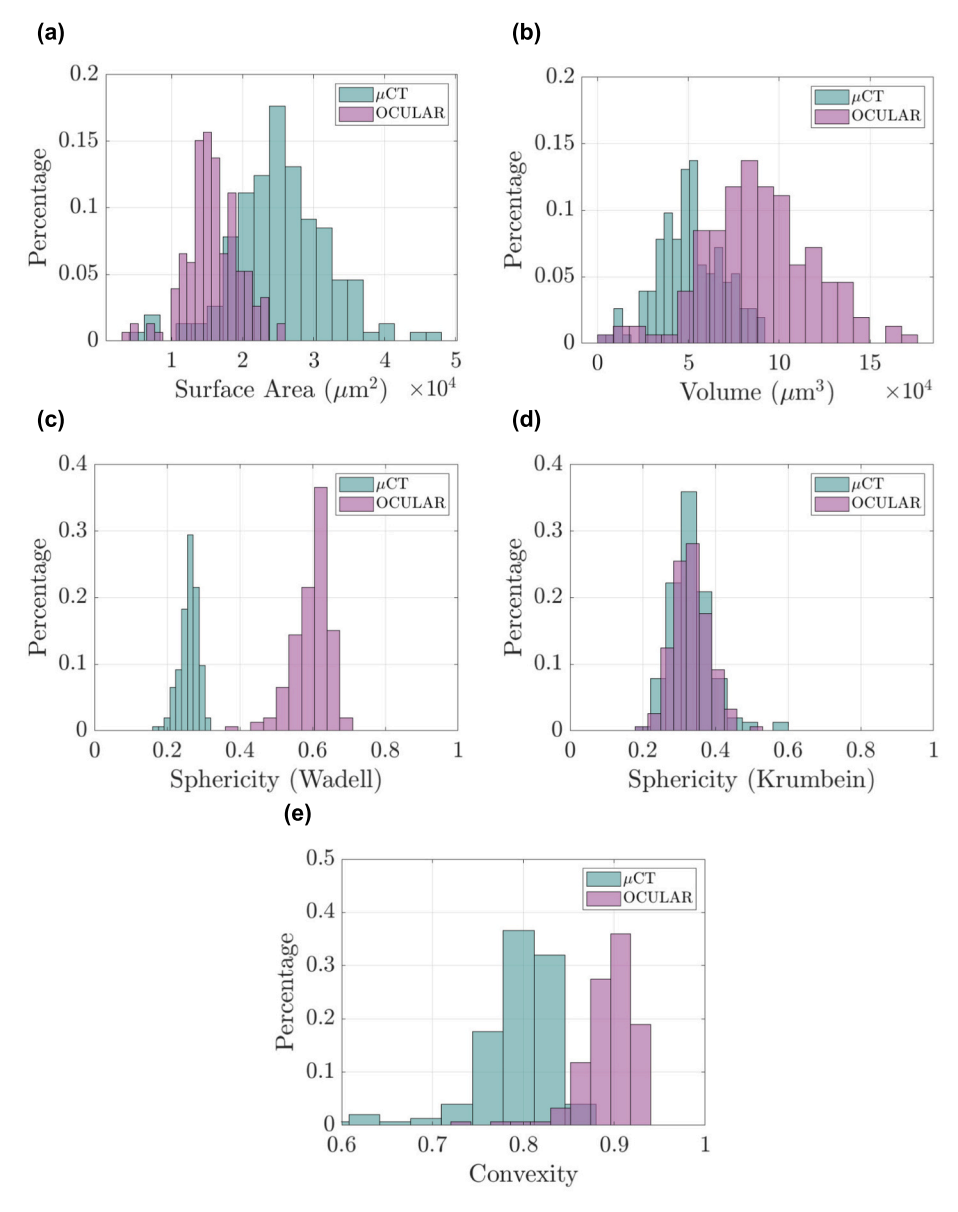


Fig. 6. Comparison of the particles (a) surface area, (b) volume, (c) true sphericity [12], (d) intercept sphericity [13], and (e) convexity obtained through μCT (teal coloured) and OCULAR (purple coloured). (For interpretation of the references to colour in this figure legend, the reader is referred to the web version of this article.)

the particles surface area for the calculations.

# 4. Concluding remarks

This paper presented OCULAR, a hardware and software solution for three-dimensional dynamic image analysis of fine particles. By addressing the limitations of traditional two-dimensional imaging, OCULAR provides a more accurate and comprehensive method for particle shape and size characterisation. Unlike existing 3D imaging techniques, which are often limited to static samples, OCULAR enables the analysis of continuously flowing particles, making it particularly suitable for high-throughput analysis. The core functionality of the OCULAR system is to capture dynamic scenes in real time manner, contributing to its suitability for high-throughput applications. Future work will explicitly explore this functionality and demonstrate its application in ultra-high speed analysis. The system ability to capture detailed 3D particle morphology through synchronised optical cameras allows for robust and real-time particle characterisation, offering significant advantages over conventional methods.

The repeatability of the OCULAR system has been validated, showing consistent results in particle size and shape distributions across multiple experimental runs. Moreover, the comparison between OCULAR and  $\mu CT$  demonstrates strong agreement in both size and shape measurements, further confirming the reliability and accuracy of the system. These findings highlight the potential of OCULAR as an efficient tool for a wide range of applications involving particles.

# CRediT authorship contribution statement

Sadegh Nadimi: Writing – review & editing, Writing – original draft, Supervision, Resources, Methodology, Investigation, Funding acquisition, Conceptualization. Vasileios Angelidakis: Writing – review & editing, Writing – original draft, Supervision, Software, Methodology, Investigation, Data curation. Sadaf Maramizonouz: Writing – original draft, Visualization, Validation, Software, Methodology, Investigation, Formal analysis, Data curation. Chao Zhang: Visualization, Validation, Methodology, Formal analysis.

# Declaration of competing interest

The first and second authors are founders and directors of OCULAR Systems Ltd. and have a patent for "Three-Dimensional Object Shape Acquisition Characterisation and Classification" (International Publication Number: WO 2023/180742). The remaining authors have no conflicts of interest to declare.

# Acknowledgments

This work was supported by the Engineering and Physical Sciences Research Council, grant number EP/R511584/1 entitled "OCULAR: Automated Acquisition and Classification of Particles" and Northern Accelerator, grant numbers: NACCF244 and NA-SPF11, entitled "OCULAR2.0: Automated Acquisition and Classification of Particles" and "OCULAR Smart Sample Presentation Unit", respectively.

# Data availability

Data will be made available on request.

#### References

- [1] R. Huang, L. Jiang, J. Zheng, T. Wang, H. Wang, Y. Huang, Z. Hong, Genetic bases of rice grain shape: so many genes, so little known, Trends Plant Sci. 18 (2013) 218–226, https://doi.org/10.1016/j.tplants.2012.11.001.
- [2] R. Suhag, A. Kellil, M. Razem, Factors influencing food powder flowability, Powders 3 (2024) 65–76, https://doi.org/10.3390/powders3010006.
- [3] P. Haftbaradaran Esfahani, R. Knöll, Cell shape: effects on gene expression and signaling, Biophys. Rev. 12 (2020) 895–901, https://doi.org/10.1007/s12551-020.00722.4
- [4] S. Abdel-Hamid, F. Alshihabi, G. Betz, Investigating the effect of particle size and shape on high speed tableting through radial die-wall pressure monitoring, Int. J. Pharm. 413 (2011) 29–35, https://doi.org/10.1016/j.ijpharm.2011.04.012.

- [5] L.M. Le Pen, W. Powrie, A. Zervos, S. Ahmed, S. Aingaran, Dependence of shape on particle size for a crushed rock railway ballast, Granul. Matter 15 (2013) 849–861, https://doi.org/10.1007/s10035-013-0437-5.
- [6] A. Tsuchiyama, T. Sakurama, T. Nakano, K. Uesugi, M. Ohtake, T. Matsushima, K. Terakado, E.M. Galimov, Three-dimensional shape distribution of lunar regolith particles collected by the Apollo and Luna programs, Earth Planets Space 74 (2022) 172. https://doi.org/10.1186/s40623-022-01737-9.
- [7] U. Ulusoy, A review of particle shape effects on material properties for various engineering applications: from macro to nanoscale, Minerals 13 (2023) 91, https://doi.org/10.3390/min13010091.
- [8] J. Fonseca, C. O'Sullivan, M.R. Coop, P.D. Lee, Non-invasive characterization of particle morphology of natural sands, Soils Found. 52 (2012) 712–722, https://doi. org/10.1016/j.sandf.2012.07.011.
- [9] S. Nadimi, J. Fonseca, Single-grain virtualization for contact behavior analysis on sand, J. Geotech. Geoenviron. Eng. 143 (2017) 06017010, https://doi.org/ 10.1061/(ASCE)GT.1943-5606.0001740.
- [10] V. Angelidakis, S. Nadimi, M. Garum, A. Hassanpour, Nano-scale characterization of particulate Iron pyrite morphology in shale, Part. Part. Syst. Charact. 39 (2022) 2200120, https://doi.org/10.1002/ppsc.202200120.
- [11] A. Jeyasountharan, K. Shahrivar, G. D'Avino, F. Del Giudice, Viscoelastic particle train formation in microfluidic flows using a xanthan gum aqueous solution, Anal. Chem. 93 (2021) 5503–5512, https://doi.org/10.1021/acs.analchem.0c05370.
- [12] V. Angelidakis, S. Nadimi, S. Utili, Elongation, flatness and compactness indices to characterise particle form, Powder Technol. 396 (2022) 689–695, https://doi.org/ 10.1016/j.powtec.2021.11.027.
- [13] T. Zingg, Beitrag zur Schotteranalyse, ETH Zurich, 1935.
- [14] V. Angelidakis, S. Nadimi, S. Utili, SHape Analyser for particle engineering (SHAPE): seamless characterisation and simplification of particle morphology from imaging data, Comput. Phys. Commun. 265 (2021) 107983, https://doi.org/ 10.1016/j.cpc.2021.107983.
- [15] H. Wadell, Volume, shape, and roundness of rock particles, J. Geol. 40 (1932) 443–451.
- [16] W.C. Krumbein, Measurement and geological significance of shape and roundness of sedimentary particles, J. Sediment. Res. 11 (1941) 64–72, https://doi.org/ 10.1306/D42690F3-2B26-11D7-8648000102C1865D.
- [17] C.O.R. Abbireddy, C.R.I. Clayton, A review of modern particle sizing methods, P I Civil Eng. -Geotec. 162 (2009) 193–201, https://doi.org/10.1680/ geng.2009.162.4.193.
- [18] E. Vigneau, C. Loisel, M.F. Devaux, P. Cantoni, Number of particles for the determination of size distribution from microscopic images, Powder Technol. 107 (2000) 243–250, https://doi.org/10.1016/S0032-5910(99)00192-8.